Photoacoustics 28 (2022) 100414

Contents lists available at ScienceDirect

Photoacoustics

journal homepage: www.elsevier.com/locate/pacs

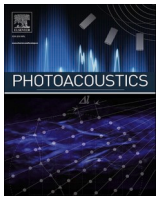

Multispectral optoacoustic tomography for the non-invasive identification of patients with severe anemia in vivo☆

Ingo Ganzleben [a,b,c], Daniel Klett [a,b,c], Wiebke Hartz [a,b,c], Lisa Götzfried [a,b,c], Francesco Vitali [a,b,c], Markus F. Neurath [a,b,c,d], Maximilian J. Waldner [a,b,c,d,*]

[a] Department of Medicine 1, University Hospital, Friedrich-Alexander-Universität Erlangen-Nürnberg, Germany
[b] Ludwig-Demling-Center for Molecular Imaging, Department of Medicine 1, University Hospital, Friedrich-Alexander-Universität Erlangen-Nürnberg, Germany
[c] Deutsches Zentrum Immuntherapie, Erlangen, Germany
[d] Erlangen Graduate School in Advanced Optical Technologies (SAOT), Friedrich-Alexander-Universität Erlangen-Nürnberg, Germany

ARTICLE INFO

Keywords:
Anemia
Hemoglobin
Optoacoustic imaging
Clinical study

ABSTRACT

The immediate diagnosis of severe anemia is crucial for patient outcome. However, reliable non-invasive point-of-care diagnostic tools for e.g., ICU monitoring are currently lacking. Using an advanced Multispectral Optoacoustic Tomography (MSOT) research device, we first substantiated a strong positive correlation of MSOT-signal and absolute hemoglobin concentration *ex vivo* in blood samples. In a clinical exploratory proof-of-concept study, we then evaluated 19 patients with different severities of anemia and controls by non-invasive in vivo measurement of hemoglobin in the radial artery. Our approach proved excellent in identifying patients with severe anemia triggering RBC transfusion based on a strong positive correlation of MSOT-signal intensity and hemoglobin concentration for 700 nm single wavelength and HbR unmixed MSOT-parameter analysis. In conclusion, our study lays the foundation to further develop MSOT-based real-time quantitative perfusion analyses in follow-up preclinical and clinical imaging studies and as a promising diagnostic tool to improve patient care in the future. DRKS00021442

1. Introduction

Severe anemia is a life-threatening condition affecting patients from almost all medical disciplines. This includes, for example, patients suffering from gastrointestinal bleeding, trauma patients with severe bleeding, patients undergoing major surgery, and an overall high percentage of patients with prolonged intensive care unit treatment. In the latter group in particular, the necessity to repeatedly draw diagnostic blood samples represents a major iatrogenic contribution to the development of anemia. Complicating matters is oftentimes the fact that severe anemia only represents one of several major medical problems in these patients, e.g., a patient with severe circulatory septic shock who is additionally severely anemic, making clinical diagnosis of anemia unreliable. While existing CO pulse oximetry devices allow non-invasive assessment of hemoglobin oxygenation (i.e., oxygen content of the blood) and in select devices total hemoglobin, they are limited by impaired arterial perfusion and perturbance variables such as bilirubin. Accordingly, without additional infrastructure, there is currently no device enabling emergency medical personnel to immediately and reliably rule out severe anemia in an unconscious patient found with compromised circulatory status outside the clinic. Furthermore, there is currently no non-invasive longitudinal monitoring system that allows detecting relevant drops in hemoglobin concentration that require transfusion during major surgery, again necessitating discontinuous monitoring with invasive blood sampling. However, identifying or ruling out severe anemia in the preclinical setting, or detecting it with low latency in the OR or ICU would improve reaction time for necessary subsequent diagnostic and therapeutic steps and improve patient care. Multispectral Optoacoustic Tomography (MSOT) is a new and promising application of the optoacoustic effect in preclinical and clinical imaging. Optoacoustic imaging (OAI) is based on the principle that pulsed laser light of a particular wavelength is specifically absorbed by molecules which thereby act as chromophores. This principle applies to exogenous chromophores [1,2] but also to endogenous molecules such as collagen [3] or hemoglobin [4], enabling label-free imaging of biological systems. Absorption of the pulsed laser energy causes cycles of molecular

☆ One Sentence Summary: A translational pilot study identifying patients with severe anemia by non-invasive hemoglobin MSOT measurement in vivo.

* Correspondence to: Department of Medicine 1, Friedrich-Alexander-Universität Erlangen-Nürnberg, Erlangen, Germany.
E-mail address: maximilian.waldner@uk-erlangen.de (M.J. Waldner).

https://doi.org/10.1016/j.pacs.2022.100414
Received 17 August 2022; Received in revised form 29 September 2022; Accepted 10 October 2022
Available online 12 October 2022

expansion and contraction, which in turn result in the emission of acoustic pressure waves. These pressure waves, which are then registered by a detector device and computed into a visual signal representation, are the basis for a quantitative analysis. Multispectral Optoacoustic Tomography (MSOT) has so far been used successfully in clinical studies evaluating malignant diseases such as breast cancer [4] or malignant melanoma [2], as well as inflammatory diseases such as Crohn's disease [5,6]. However, these studies used MSOT signal data either for visual representation of structures such as cancerous lesions [4], or they used MSOT signal intensity for hemoglobin in tissues as a surrogate parameter for disease activity based on its positive correlation with increased perfusion that is associated with acute inflammation [5,6]. Given the vast potential of the technology platform in combination with recent advances in spectral unmixing approaches [7,8], we decided

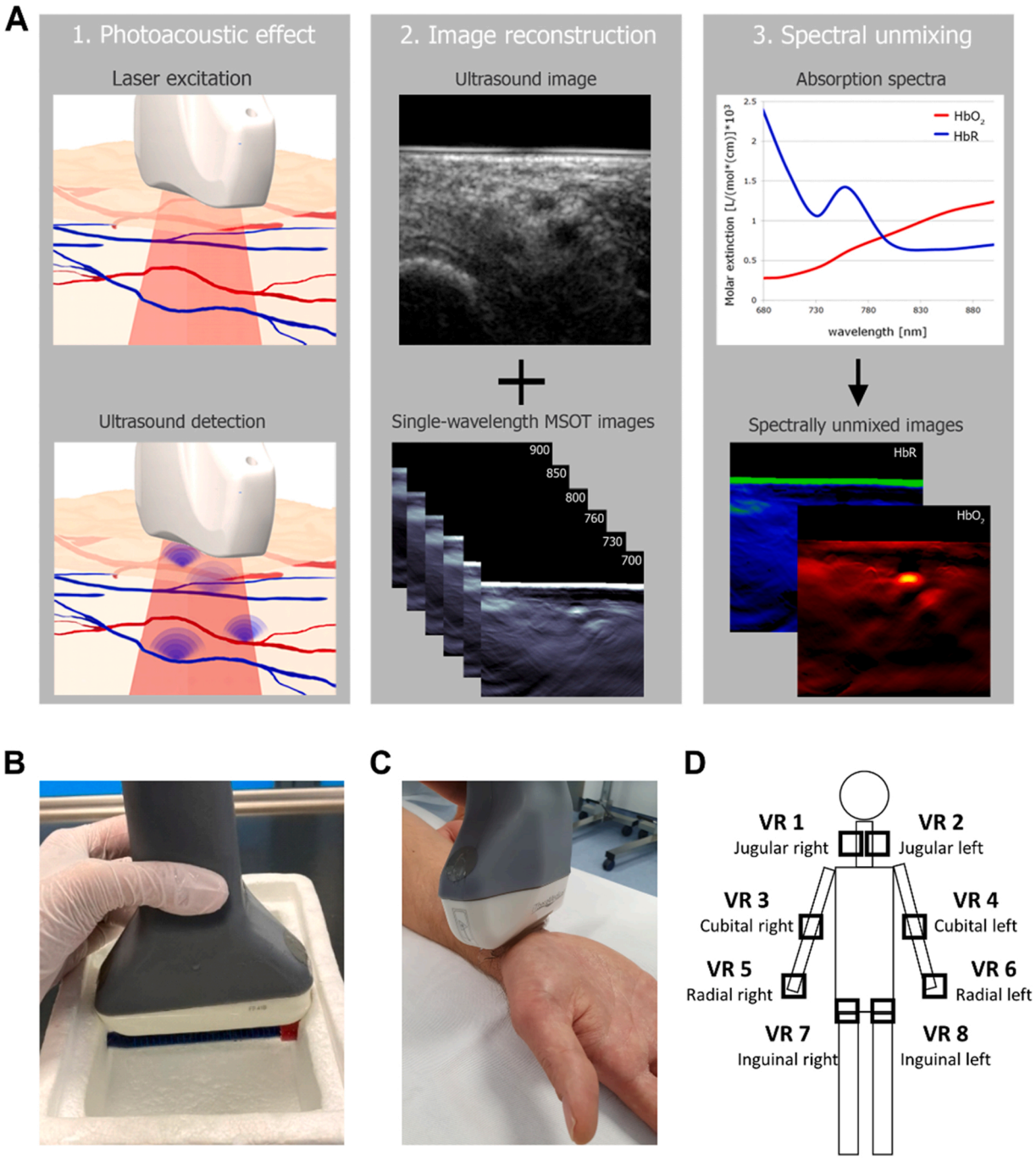

Fig. 1. Basic principles and setup of multispectral optoacoustic tomography (MSOT). (A) Graphic depiction of the multispectral optoacoustic measurement (MSOT) principle. 1.) Light pulses intermittently transfer energy to the hemoglobin molecule resulting in cycles of heating/cooling with subsequent alternating expansion/contraction. This results in detectable ultrasound pressure waves. 2.) In a next step, reflectance ultrasound images are acquired interleaved with single wavelength images in a range of 700–900 nm. 3.) Spectral unmixing based on the absorption spectra of the target molecules enables a molecule-centric view of e.g., deoxyhemoglobin (HbR). (B) Representative photography of an MSOT Acuity Echo research system *ex vivo* sample measurement using the handheld 2D probe on a placeholder sample. Samples were kept in a 15 ml transparent polypropylene (PP) container, which was placed in ultrapure water as coupling medium. (C) Representative photography of an MSOT Acuity Echo research system in vivo measurement of the right radial artery using the handheld 2D probe. (D) MSOT measurements were performed systematically on eight vascular regions (VR 1 – VR 8) as illustrated.

to evaluate the quantitative relationship between relevant single wavelength and spectrally unmixed parameters and hemoglobin concentration. Our primary aim was to evaluate if measurements using an advanced MSOT clinical research device might be capable of noninvasive identification of patients with severe anemia in an exploratory translational proof-of-concept study. By establishing optoacoustic hemoglobin quantification in vivo as a potential diagnostic tool for anemia, we hope to lay the foundation to improve patient care by providing prompt and reliable results in situations such as emergency medical care when no lab analysis is available or in the ICU for longitudinal monitoring and by refining optoacoustic imaging in diseases such as cancer in the future.

2. Materials and methods

2.1. Basic principles and setup of multispectral optoacoustic tomography (MSOT)

Multispectral optoacoustic tomography (MSOT) was conducted using a commercial multispectral optoacoustic imaging tomograph (MSOT Acuity Echo research system, iThera Medical GmbH, Germany) on ex vivo samples and subsequently in vivo in patients with anemia and normal hemoglobin levels. As illustrated in Fig. 1A, the MSOT principle is based on the photoacoustic effect and takes advantage of the specific absorption wavelengths of particular target molecules such as hemoglobin. In short, the hemoglobin molecules take up energy provided by the laser source of the device at specific wavelengths. The following cycle of molecular expansion and re-condensation creates pressure waves, which are in turn detected by the handheld detector probe. While the absorption properties of hemoglobin depend on its oxygenation status, absorption at the isosbestic point of hemoglobin at 800 nm is reflective of overall hemoglobin (both oxygenated and deoxygenated). The MSOT image reconstruction generates an ultrasound image and single wavelength analyses. Beyond that, based on the absorption spectra of molecules such as deoxyhemoglobin (HbR) and oxyhemoglobin (HbO_2), a spectral unmixing of the MSOT signal was performed resulting in molecule-specific quantitative information (Fig. 1A). In our current study, we first employed MSOT imaging ex vivo based on a measurement setup illustrated in Fig. 1B, using the handheld 2D probe on samples in a 15 ml polypropylene container placed in ultrapure water as coupling medium. Fig. 1C and 1D illustrate the measurement setup and protocol of the subsequent in vivo study, showing a representative photography of an in vivo measurement of the right radial artery using the handheld 2D probe (Fig. 1C) and the systemic evaluation of eight defined vascular regions (VR 1 – VR 8, Fig. 1D).

2.2. Multispectral optoacoustic tomography (MSOT) and data analysis

For MSOT imaging, a hybrid optoacoustic/ultrasound imaging system was used (MSOT Acuity Echo research imaging system with 2D detector probe, iThera Medical GmbH, Munich, Germany). Briefly, a tunable optical parametric oscillator (OPO) pumped by an Nd:YAG laser provides excitation pulses with a duration of 9 ns at wavelengths from 660 nm to 1300 nm at a repetition rate of 25 Hz with a wavelength tuning speed of 10 ms. The pulse energy is attenuated to ensure adherence with ANSI limits of maximum permissible exposure (MPE). For ultrasound detection, 256 ultrasound transducers with a center frequency of 4 MHz (60% bandwidth), organized in a concave array of 125-degree angular coverage and a radius of curvature of 4 cm are used. A reflectance ultrasound computed tomography (RUCT) unit was integrated in the system for ultrasound background image. While single wavelengths constitute the combined absorption of all molecules of a sample at this particular wavelength, spectrally unmixed parameters allow for a specific molecule-centric view. In particular, spectral absorption characteristics of hemoglobin depend on its oxygenation status i.e., whether it exists as deoxygenated hemoglobin (HbR) or oxygenated hemoglobin (HbO_2). Single wavelength absorption peaks for hemoglobin within the available spectrum of the MSOT Acuity research device in the near-infrared range (660–1300 nm) are at 760 nm for HbR and 900 nm for HbO_2. The absorption of both HbR and HbO_2 is identical at 800 nm, the isosbestic point, therefore correlating with the total amount of hemoglobin (HbT). In this study, optoacoustic signals from 700 nm, 730 nm, 760 nm, 780 nm, 800 nm, 850 nm and 900 nm were collected. Backprojection algorithm was used to reconstruct the images. To increase signal-to-noise ratio, signal was averaged over 7 consecutive laser pulses for each wavelength. Linear regression algorithm was used to spectrally unmix for oxyhemoglobin (HbO_2) and deoxyhemoglobin (HbR). Additionally, the composite measurement parameter total hemoglobin (HbT), which represents the sum of HbR and HbO_2, was calculated.

For quantifying the MSOT signal, a region-of-interest (ROI) was drawn and the mean optoacoustic signal intensity in the ROI was quantified. In detail, following export from the MSOT Acuity Echo research imaging system, ROI demarcation was performed using the cLabs software (version 2.69, iThera Medical). For ex vivo samples, unless noted otherwise, individual region-of-interest polygons (ROI_{visual}) were determined by a researcher in a non-blinded fashion for each sample based on the visual representation of the signal intensity at 800 nm. Selected analyses, e.g., when no visual signal was discernable, used a standardized ROI encompassing up to half of the depth of the sample container, or as for comparison experiments the complete inner area of the sample container regardless of visual signal ($ROI_{standard}$).

ROIs for in vivo measurements of the radial vascular regions were drawn around the specific vascular target structure i.e., the radial artery using the ultrasound image (RUCT) in a blinded-fashion. ROIs for the other vascular regions were drawn in a similar but non-blinded fashion as described in Fig. S5.

2.3. Preparation and measurement of ex vivo samples

All samples were measured in transparent standard 15 ml polypropylene (PP) sample containers (62.554.502, Sarstedt) which were submerged manually in ultrapure water (Synergy UV, Merck Millipore) as coupling medium. Data recording and processing was performed via the viewMSOT software on the MSOT Acuity echo research device.

Unless noted otherwise, all samples were measured longitudinally with direct contact between the detector surface and the sample container facilitated by the coupling medium. In selected measurement series, this setup was altered to allow a distance of about 0.5–1 cm in between the detector surface and the sample container within the coupling medium. Adequate positioning was verified using the RUCT image of the MSOT Acuity research device.

2.3.1. Blood dilution series

EDTA-anticoagulated blood samples were diluted to achieve a fine-grained dilution series with variable hemoglobin concentrations. Unless indicated otherwise, plasma isotone saline (NaCl 0.9%) was used as dilution medium. In selected measurement series, ultrapure water (Synergy UV, Merck Millipore) was used for dilution as indicated. In principle, the undiluted blood sample was measured for hemoglobin concentration using a blood gas analysis device (ABL800 FLEX/ ABL90 FLEX in combination with Arterial Blood Sampler PICO50, 956–552, both Radiometer). Based on the hemoglobin concentration, the necessary dilution steps were calculated with the following formulas:

$$X = \frac{Hu}{HT}$$

X = dilution quotient
H_u = undiluted hemoglobin concentration [g/dl]
H_T = target hemoglobin concentration [g/dl]

$$VB = \frac{VT}{X}$$

V_B = blood volume [ml]
V_T = target total volume [ml]
X = dilution quotient

$$VD = VT - VB$$

V_D = dilution medium volume [ml]
V_T = target total volume [ml]
V_B = blood volume [ml]

For target hemoglobin concentrations of up to 10 g/dl, a parallel dilution was performed as stated above, while target hemoglobin concentrations above 10 g/dl were achieved via serial dilution.

$$X = \frac{HP}{HT*}$$

X = dilution quotient.
H_P = hemoglobin concentration of previous sample [g/dl].
H_T * = target hemoglobin concentration of next step in dilution series [g/dl].

Each sample was then again validated via gold standard measurement (blood gas analysis) with a mean latency of 15 min (minimum: 5 min, maximum: 62 min) to the MSOT measurement and the actual hemoglobin concentration was used for further analyses. Cumulative data of several experiments were analyzed and served as training data for the fitting of a standard curve as indicated in the respective figure legends. An additional experiment was then assessed in blinded fashion and used as test data to interpolate hemoglobin values based on MSOT signal intensity. Results from ultrapure water-based dilutions were obtained in analogue fashion with a mean latency of 40 min (minimum: 4 min, maximum: 68 min).

2.4. Patient measurements in vivo

After informed consent, patients were positioned on an examination table in prone position. MSOT measurements were performed under standard precautions, including safety goggles, on eight vascular regions (VR) in the following order for each patient: VR1 (jugular right), VR2 (jugular left), VR3 (cubital right), VR4 (cubital left), VR5 (radial right), VR6 (radial left), VR7 (inguinal right), and VR8 (inguinal left). Aquasonic clear ultrasound gel (#03–08, Parker Laboratories Inc.) was used as coupling medium.

2.5. Study approval and clinical study design

The study was approved by the ethics committee of the University of Erlangen-Nürnberg (64_20 B) and registered at the German Clinical Trials Register (Identifier: DRKS00021442; Universal Trial Number

Table 1 –
Patient characteristics.

Study ID	Hemoglobin [g/dl]	Hematocrit [%]	Age [years]	Sex	Assumed main cause of anemia	Relevant diagnoses
	Severe anemia (< 8 g/dl)					
MERIT 7	4.5	15.6	42	w	not available	not available
MERIT 20	4.5	15.2	65	w	Hemorrhagic (upper GI-bleeding)	suspected malignant tumor (nodule of the adrenal gland), thyroid nodule, S/P breast cancer, S/P resection of a melanoma
MERIT 19	6.2	19.5	58	m	Hemorrhagic (upper GI-bleeding)	chronic pancreatitis, S/P portal vein thrombosis, diabetes mellitus type 3, CAD, HTN
MERIT 6	6.5	19.6	70	w	not available	spontaneous bacterial peritonitis (SBP), pancreatic cancer, acute kidney failure, UTI, S/P breast cancer, hypothyroidism
MERIT 5	7.1	20	57	w	not available	liver cirrhosis, esophageal varices (grade 1), S/P Waldenstrom's disease, HTN, hypothyroidism
MERIT 4	7.6	22.5	65	w	Hemorrhagic (upper GI-bleeding)	liver cirrhosis, acute-on-chronic kidney failure, UTI, hypothyroidism, diabetes mellitus type 2
	Non-severe anemia (≥ 8 g/dl; < LLN)					
MERIT 8	8.1	25.4	48	w	Hemorrhagic (upper GI-bleeding)	primary sclerosing cholangitis, ulcerative colitis (pancolitis), S/P iatrogenic pancreatitis with acute kidney failure, erysipelas, sarcoidosis, Basedow's disease
MERIT 17	8.6	25.7	58	m	not available	hepatocellular carcinoma, liver cirrhosis, chronic kidney failure, hypothyroidism, diabetes mellitus type 2, HTN
MERIT 11	9	30	23	w	iron-deficiency anemia	ulcerative colitis, S/P pulmonary embolism
MERIT 1	9.4	29.1	42	w	iron-deficiency anemia	ulcerative colitis
MERIT 2	9.4	28	66	m	Hemorrhagic (upper GI-bleeding)	portal vein thrombosis, esophageal varices
MERIT 13	9.5	28.4	54	w	folate/vitamin B12 deficiency anemia	common bile duct stenosis, S/P neuroendocrine tumor (NET) of the pancreas, HTN
MERIT 12	10.1	29.8	75	m	not available	hepatocellular carcinoma, liver cirrhosis, diabetes mellitus type 2, HTN, coronary artery disease, S/P MI, obesity
	Normal range (≥ LLN; ≤ ULN)					
MERIT 9	13.3	38.9	23	w	not applicable	Crohn's disease
MERIT 10	13.9	40.7	25	m	not applicable	cystic fibrosis
MERIT 18	14.5	42.5	35	m	not applicable	hepatitis E (acute)
MERIT 3	15	46.4	57	m	not applicable	COPD, pulmonary nodule
MERIT 16	15.2	44.8	48	m	not applicable	hypercalcemia, sarcoidosis, acute-on-chronic kidney failure, HTN, diabetes mellitus (secondary to GC), cholecystolithiasis, hepatic steatosis, obesity
MERIT 14	16.2	48.9	73	m	not applicable	urosepsis, HTN, PLMD, CAD, S/P aortic valve replacement, A-fib, S/P concealed perforated sigmoid diverticulitis, diabetes mellitus type 2, hyperuricemia, CIP

S/P status post, CAD coronary artery disease, UTI urinary tract infection, HTN arterial hypertension, GC glucocorticoids, PLMD Periodic-Limb-Movement-Disorder, A-fib atrial fibrillation, CIP critical illness neuropathy, LLN lower level of normal

(UTN): U1111–1250–5212). Inclusion criterion was age $\geq$ 18 years. Exclusion criteria were age below 18 years, pregnancy, and/or mental retardation* of the patient with restriction of general judgment and awareness. In the period from July 9th, 2020 to October 21st, 2020 overall 20 patients were recruited after giving informed written consent. One patient had to be excluded due to a running lipid infusion for parenteral nutrition, as the absorption wavelength of the contained lipids interfered with our intended analysis. In total, a study population of 19 patients (9 male, 10 female) was included in the analysis. An overview of the patient characteristics is given in Table 1. Study recruitment was conducted among patients fulfilling the inclusion criterion based on their respective laboratory determined hemoglobin concentration measured in context of their routine care. Patients were recruited into two main groups "normal (n = 6)" which included hemoglobin concentrations $\geq$ the lower limit of normal (LLN) and $\leq$ the upper limit of normal (ULN) and "anemia" (n = 13) which included patients with a hemoglobin concentration below the LLN. During data analysis, subgroup analysis was performed resulting in the anemia subgroups of "non-severe anemia" (n = 7) (Hb $\geq$ 8.0 g/dl; <LLN) and "severe anemia" (n = 6) (Hb < 8.0 g/dl). Directly before or after the MSOT measurement, an additional venous blood sample was drawn and the hemoglobin concentration was determined by laboratory analysis (gold standard analysis).

* Exact terminology as used in the original ethics approval filing stemming from the German in-use medical term "Mentale Retardierung". Based on DSM-5 the relevant English term is "intellectual disability".

2.6. Statistical analysis

Comparisons between two groups were performed using unpaired or paired parametric t-test depending on the data as indicated in the specific figure legends. Comparisons of three groups were performed using One-Way ANOVA (Analysis of Variance) with Tukey's test as post hoc test as indicated in the specific figure legends. Data sets are displayed as one of the following: interleaved scatter of individual values with mean, single values, Tukey's box plot (box from 25th to 75th percentile, line represents median; whiskers according to Tukey's method) or truncated violin plots with additional depiction of single values as indicated in the specific figure legends. Statistical significance was accepted with $p < 0.05$ (ns $p \geq 0.05$; *$p < 0.05$; **$p < 0.01$; ***$p < 0.001$; ****$p < 0.0001$). All p values calculated using Tukey's test are given as multiplicity adjusted p values. Standard curve fitting was performed using a hyperbola or a sigmoidal curve-fitting approach as appropriate. Correlation analysis was performed calculating Spearman's rank correlation coefficient with the 95% confidence interval or Pearson's correlation coefficient (r) with a 95% confidence interval as well as the coefficient of determination (R^2) as appropriate. Receiver operating characteristic (ROC) were calculated with determination of the Area under the ROC curve (AUROC), the 95% confidence interval, and the significance level. A post hoc power analysis was performed to compute the achieved power. Statistical calculations were performed using GraphPad Prism 8/9 (GraphPad Software Inc.) and GPower 3.1 [9,10].

2.7. Software

Software used in the data analysis, data processing, and preparation of the manuscript included cLabs Software v2.69 and iLabs Software (both iThera Medical, Munich), Microsoft Office (Excel, Word, PowerPoint; Microsoft), GraphPad Prism 8/9 (GraphPad Software Inc.), GPower 3.1 [9,10], and Affinity Designer (Serif (Europe) Ltd).

3. Results

3.1. MSOT-based hemoglobin detection allows semi-quantitative analysis of hemoglobin in diluted blood samples ex vivo

First, we performed a detailed analysis of hemoglobin concentration [g/dl] and MSOT signal intensity [au] by employing a fine-grained dilution series of EDTA-anticoagulated whole blood plasma in isotone saline for ex vivo measurement (Fig. 2). In an initial assessment, we found that the MSOT signal intensity at multiple single wavelengths including 700 nm, 800 nm, and 900 nm increased with increasing hemoglobin concentration as measured by our gold standard laboratory analysis in form of a blood gas analysis measurement (Fig. 2A). In a first quantitative analysis, all blood dilution samples that fell within $\pm$ 0.3 g/dl of integral hemoglobin concentrations (e.g., 1 g/dl) according to their blood gas analysis result were grouped and plotted against their MSOT signal level at 800 nm as shown in Fig. 2B. The results were in accordance with the visual signal representation (Fig. 2A) and demonstrated that quantitative MSOT signal levels at 800 nm did indeed positively correlate with absolute hemoglobin concentration. Next, we performed a more detailed analysis using all available dilution samples i.e., also including samples that did not, due to variations in the dilution process, fall within the defined $\pm$ 0.3 g/dl corridor, to analyze the relationship between MSOT signal level and hemoglobin concentration (Fig. 2C-J). Curve fitting using a hyperbola approach in combination with a correlation analysis resulted in a significant positive non-linear monotonic correlation of hemoglobin [g/dl] and MSOT signal level [au] at 800 nm (Spearman r 0.9922; 95% CI [0.9837–0.9939], ****$p < 0.0001$; Fig. 2C), with an almost identically high level of correlation for the spectrally unmixed composite parameter HbT (Spearman r 0.9901; 95% CI [0.9820–0.9946], ****$p < 0.0001$; Fig. 2D). Extended spectral analysis of 700 nm (Spearman r 0.9595; 95% CI [0.9273–0.9776], ****$p < 0.0001$; Fig. 2E) and HbR (Spearman r 0.9463; 95% CI [0.9041–0.9702], ****$p < 0.0001$; Fig. 2F), as well as 900 nm (Spearman r 0.9924; 95% CI [0.9862–0.9958], ****$p < 0.0001$; Fig. 2G) and HbO_2 (Spearman r 0.9812; 95% CI [0.9660–0.9897], ****$p < 0.0001$; Fig. 2H) proved to be in the same excellent range and strongly positively correlated with hemoglobin concentration. In summary, all single wavelengths and unmixed MSOT parameters displayed a strong positive correlation with the hemoglobin concentration as determined by our gold standard analysis. Overall, signal intensity at 800 nm and 900 nm had the highest level of correlation with hemoglobin concentration, with the associated spectrally unmixed MSOT parameters, the composite parameter total hemoglobin HbT and HbO_2, performing only marginally worse. Interestingly, with a Spearman correlation of r 0.9595, the single wavelength read-out of 700 nm and its associated unmixed parameter HbR (Spearman r 0.9463) representing deoxygenated hemoglobin were not relevantly worse regarding correlation with hemoglobin concentration.

Due to the novelty of our approach to use the MSOT Acuity Echo research system for absolute hemoglobin assessment, we also focused on how technical variables of the measurement process might affect analysis outcome ex vivo. With no anatomical structures in the reflectance ultrasound computed tomography (RUCT), we compared two approaches to define the ROI using a subset of the samples used in the data included in Fig. 2 (Fig. S1). Individually drawn ROIs for each sample based on the visual representation of the MSOT signal at 800 nm (ROI_{visual}) defined our standard approach with a standardized ROI encompassing the complete measurement container $ROI_{standard}$ as alternative. Of note, in samples not yielding a discernable visual signal, the ROI was drawn to the middle line of the measurement container depth in the ROI_{visual} group as this reflected the maximum extent of signal observed in samples with positive visualization (Fig. S1A). While a pooled comparison of MSOT signal levels in this subgroup showed a significantly reduced absolute MSOT signal in the $ROI_{standard}$ group (Fig. S1B), separate correlation analyses for both approaches found no

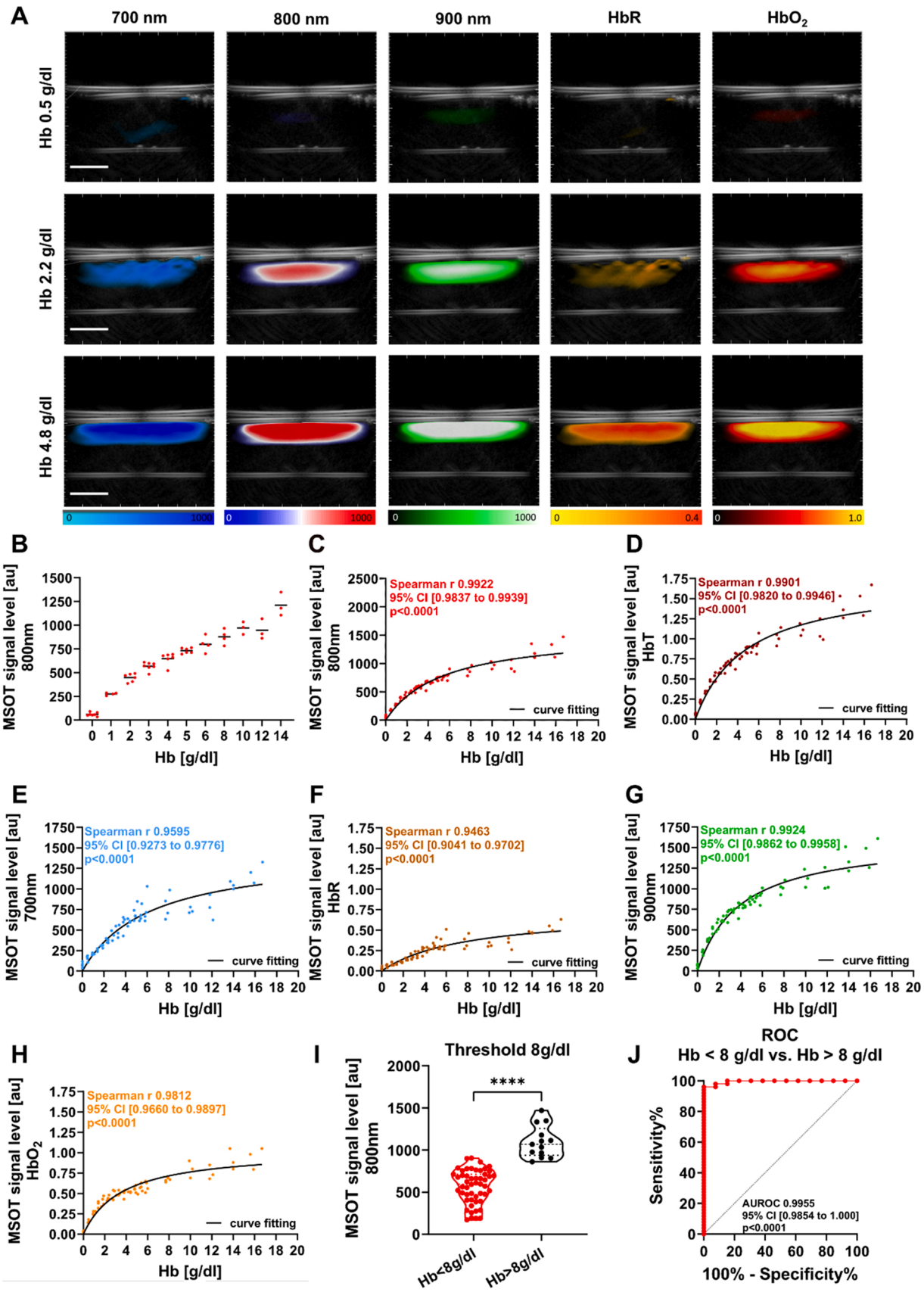

(caption on next page)

Fig. 2. MSOT-based hemoglobin detection allows semi-quantitative analysis of hemoglobin in diluted blood samples ex vivo. All hemoglobin concentrations and MSOT values represent individual measurements. (A-I) Graphic depiction of MSOT measurement data for blood samples diluted in plasma isotone saline with increasing hemoglobin concentrations as indicated. (A) Figure displays overlay images of RUCT and a color-coded representation of the MSOT signal intensity [au] for single wavelengths (700 nm, 800 nm, 900 nm) and unmixed MSOT parameters (HbR, HbO_2) in blood samples diluted with plasma isotone saline (0.9% NaCl) resulting in different hemoglobin concentrations as indicated. Samples were measured ex vivo with the MSOT Acuity 2D probe as illustrated in Fig. 1B. The region-of-interest (ROI) was individually drawn based on the MSOT signal visualization at 800 nm for reference. MSOT signal intensity increases with increasing hemoglobin concentration (Hb 0.5 g/dl, Hb 2.2 g/dl, Hb 4.8 g/dl) which was determined using blood gas analysis. Scale bar (white) indicates 10 mm. (B) Quantitative analysis of MSOT signal intensity at 800 nm [au] in a dilution series of blood diluted in plasma isotone saline (0.9% NaCl) on the y-axis. Shown are cumulative results from at least 3 independent experimental iterations with the number of measurements for each hemoglobin concentration being (Hb 0 g/dl: n = 7; Hb 1 g/dl: n = 4; Hb 2 g/dl: n = 6; Hb 3 g/dl: n = 7; Hb 4 g/dl: n = 6; Hb 5 g/dl: n = 6; Hb 6 g/dl: n = 4; Hb 8 g/dl: n = 4; Hb 10 g/dl: n = 3; Hb 12 g/dl: n = 3; Hb 14 g/dl: n = 3). Data are shown as interleaved scatter of individual values with mean. x-axis shows hemoglobin concentration from 0 to 14 g/dl in 1 g/dl intervals. All values within a range of ± 0.3 g/dl in blood gas analysis of each respective hemoglobin concentration step were included. (C-H) Graphic depiction of MSOT derived measurement parameters. Displayed are a single wavelength analysis and its corresponding spectrally unmixed MSOT parameter analysis for (C, D) 800 nm / HbT, (E, F) 700 nm / HbR, and (G, H) 900 nm / HbO_2 on each y-axis [au] against the increasing hemoglobin concentration [g/dl] of blood samples diluted in plasma isotone saline on the x-axis. Each graph displays single values of the respective parameters for all samples (n = 71, 4 experiments) with an interpolated standard curve based on a hyperbola approach in combination with a correlation analysis of [Hb (g/dl)] and the respective [MSOT signal level (au)]. The analysis for 800 nm resulted in Spearman r 0.9922; 95% CI [0.9837–0.9939], $p < 0.0001$. HbT Spearman r 0.9901; 95% CI [0.9820–0.9946], ****$p < 0.0001$. 900 nm Spearman r 0.9924; 95% CI [0.9862–0.9958] ****$p < 0.0001$. HbO_2 Spearman r 0.9812; 95% CI [0.9660–0.9897], ****$p < 0.0001$. 700 nm Spearman r 0.9595; 95% CI [0.9273–0.9776], ****$p < 0.0001$. HbR Spearman r 0.9463; 95% CI [0.9041–0.9702], ****$p < 0.0001$. (I) Graphic depiction of MSOT signal level [au] at 800 nm on the y-axis and diluted blood samples grouped on the x-axis based on a threshold hemoglobin concentration of 8 g/dl. Data are shown as truncated violin plot with depiction of individual values except blank values (i.e., hemoglobin concentration of 0 g/dl) resulting in n = 51 for Hb < 8 g/dl; n = 13 for Hb > 8 g/dl). Statistical analysis by unpaired t-test (****$p < 0.0001$; Power (1- β err prob) > 0.99). **(J)** Receiver operating characteristic (ROC) for the identification of hemoglobin concentrations below the threshold of 8 g/dl (n = 51) vs. above the threshold (n = 13) using the MSOT signal level [au] at 800 nm. Also given are the Area under the ROC curve (AUROC) with the 95% confidence interval.

significant difference but only a moderate deterioration of strength of correlation (Fig. S1C). We then evaluated the influence of a variable distance of our sample container from the detector probe surface in a different subset of our samples (Fig. S1D). While the overall difference of MSOT signal levels between the two pooled groups "proximity" (standard) and "distance" resulted in a statistically significant difference (****$p < 0.0001$) (Fig. S1E), correlation analyses again revealed only a minor deterioration for the "distance" approach (Fig. S1F). Similarly, we found using ultrapure water as dilution medium resulted in lower MSOT signal levels compared to plasma isotone saline but no relevant difference in their correlation with hemoglobin concentration as determined in our gold standard measurement (Fig. S2).

Based on these findings, we used the data acquired in our blood dilution series experiments (displayed in Fig. 2C) as training data set and its derived standard curve as basis to interpolate the hemoglobin concentration of samples based on their MSOT signal intensity at 800 nm (Fig. S3A). We then used the MSOT signal levels [au] of an independent test data set of blood diluted in plasma isotone saline which was analyzed in a blinded fashion, to interpolate the corresponding hemoglobin concentration values (Fig. S3A). Strikingly, the training data set allowed reliable and accurate interpolation of the hemoglobin concentration in unknown test samples of diluted blood with only minor to moderate differences (Fig. S3A, B, C).

To evaluate the potential usefulness of our approach in a clinical setting, we compared MSOT signal levels [au] at 800 nm below and above a threshold of a hemoglobin concentration of 8 g/dl, as this is in multiple clinical guidelines a threshold triggering the indication for a red blood cell transfusion in patients due to the severity of anemia. We found not only a highly significant difference between the two groups (p ****<0.0001; Fig. 2I) but also an excellent receiver operating characteristic (AUROC 0.9955; 95% CI [0.9854–1.000]; ****$p < 0.0001$; Fig. 2J).

3.2. MSOT imaging of hemoglobin in multiple vascular regions in vivo

In a first step to translate our promising findings into a potential clinical application, we devised a pilot study protocol evaluating the capability of the MSOT technology to identify patients with anemia, a reduced amount of hemoglobin, in vivo (Fig. 3). Based on their documented laboratory-determined hemoglobin concentrations, our gold

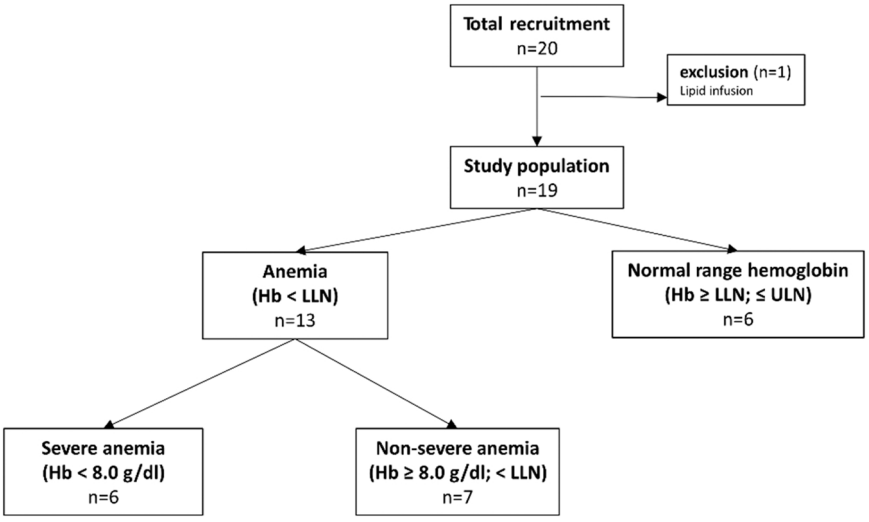

Fig. 3. Study protocol "Multispectral optoacoustic tomography for the evaluation of hemoglobin concentration in vivo trial" (MERIT). Flow chart illustrating the recruitment process and the resulting study groups.

standard analysis, we recruited a total of 20 patients of which one patient had to be excluded due to an active lipid infusion during the MOST measurement procedure. Our final study population consisted of 19 patients including 13 patients with anemia (Hb < LLN) and a control group of 6 patients with hemoglobin in the normal range (Hb ≥ LLN, Hb ≤ ULN). The subgroup analysis of the anemia group devised patients as having "severe anemia" (n = 6) when they had a hemoglobin concentration below 8.0 g/dl derived from the "transfusion threshold" triggering a red blood cell transfusion in anemic patients. Patients with a hemoglobin of less than the LLN but more than 8.0 g/dl were considered to have "non-severe anemia" (n = 7). As exemplified by a photography of a measurement of the right radial artery illustrated in Fig. 1C and D, we systematically examined eight vascular regions (VR) including the jugular, cubital, radial, and inguinal region on both sides of each patient for a total of 16 measurements per patient. At each measurement site, the RUCT images were used to focus on vascular structures such as e.g., the radial artery and to devise a region-of-interest (ROI). Representative examples of RUCT images and corresponding MSOT signal at 700 nm (single wavelength) and HbR (unmixed MSOT parameter) are shown in Fig. 4.

3.3. *Multispectral optoacoustic tomography for the non-invasive detection of severe anemia in vivo*

The radial vascular region proved to be the most promising due to the superficial position of the radial artery. Strikingly, we were able to identify the radial artery in all 19 patients and visual representation of the MSOT signal intensity at 700 nm and for HbR reflected differing signal intensities based on the hemoglobin concentration in the blood of the respective patient. Table 1 gives an overview of the patient characteristics. Fig. 5A shows a representative visualization of the radial artery of a patient with a normal hemoglobin concentration compared to a patient with severe anemia. Accordingly, we performed a quantitative analysis of the data obtained in the vascular regions 5 and 6 of the patients (Fig. 5 and Fig. S4). We found that the spectrally unmixed parameter quantifying deoxyhemoglobin (HbR) proved excellent in identifying patients with severe anemia (Fig. 5B-E). Comparative analysis of the MSOT signal [au] for HbR showed it to be significantly lower in patients with severe anemia than in control patients including normal range hemoglobin and non-severe anemia patients (***$p < 0.001$; Fig. 5B). Importantly, subgroup analysis using one-way ANOVA with Tukey's test allowed distinguishing severely anemic patients reliably from patients with a milder form of anemia (non-severe anemia,

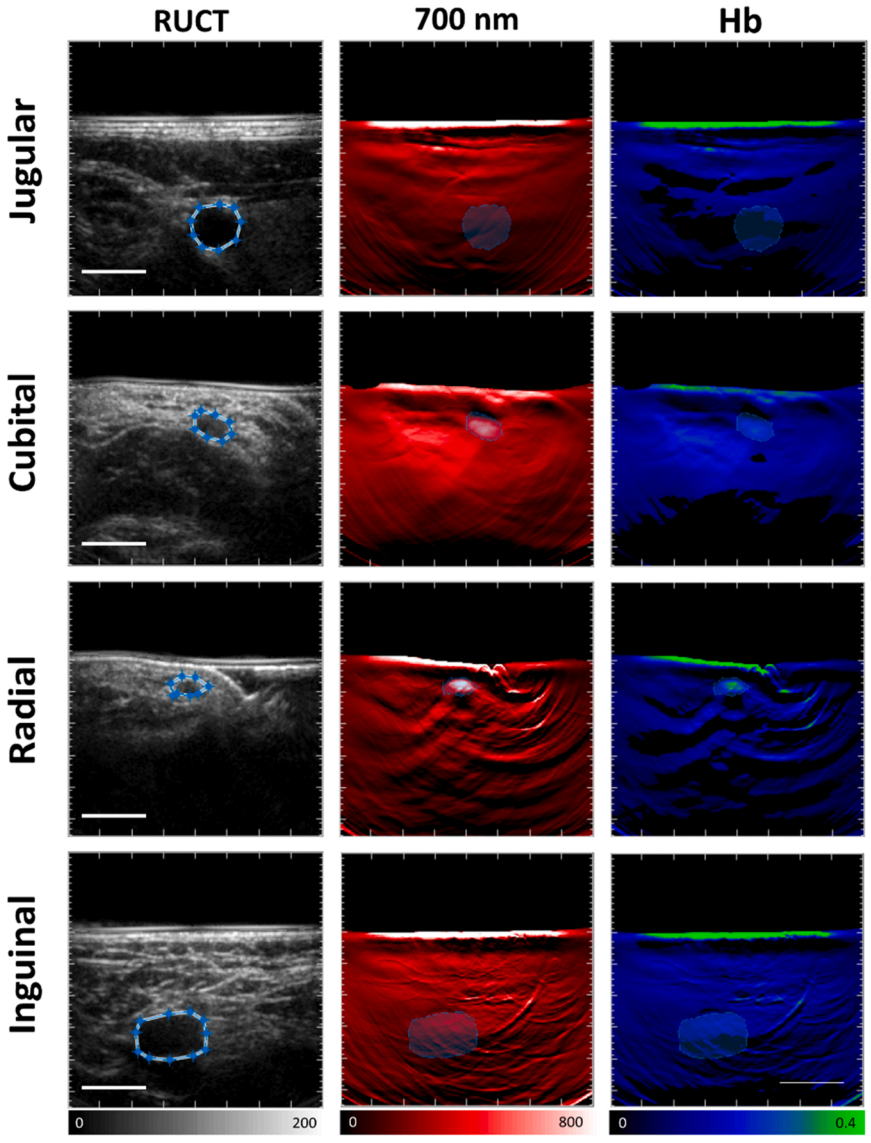

Fig. 4. MSOT imaging of hemoglobin in multiple vascular regions in vivo. Representative MSOT in vivo measurement images of different vascular regions as indicated. Scale bar (white) indicates 10 mm. First column: RUCT image ("RUCT"); second column: overlay of RUCT and color-coded signal visualization of MSOT signal at 700 nm ("700 nm", single wavelength); third column: overlay of RUCT and color-coded signal visualization of MSOT signal for HbR ("Hb", unmixed MSOT parameter). Regions-of-interest (ROIs, blue-dotted white line) were drawn to fit the vascular structure in the RUCT image.

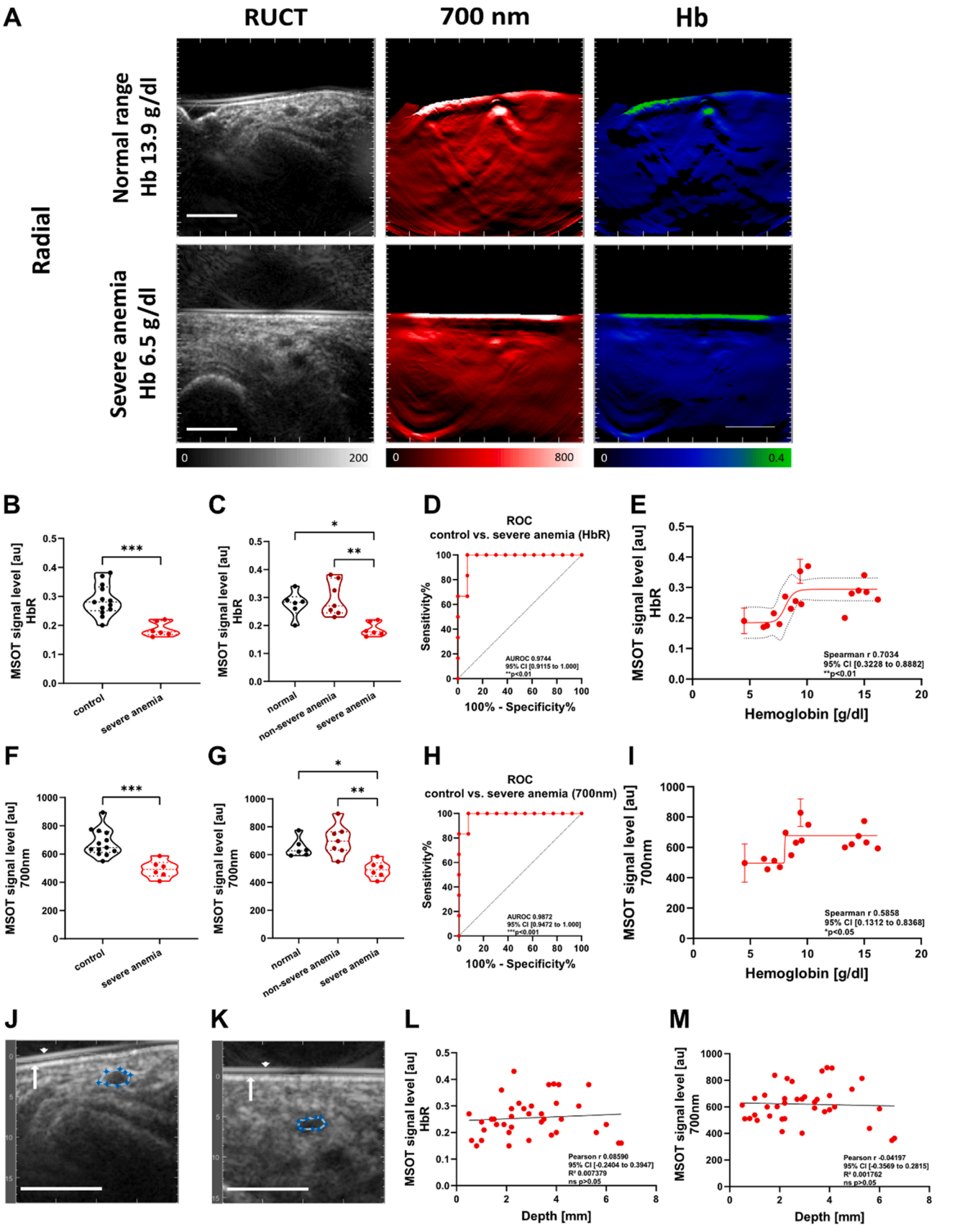

(caption on next page)

Fig. 5. Multispectral optoacoustic tomography for the non-invasive detection of severe anemia in vivo. (A) Representative MSOT in vivo measurement images of the radial artery (VR5/VR6) of two patients. Displayed are a patient with a hemoglobin concentration in the normal range (Hb 13.9 g/dl; upper row) and a patient with severe anemia (Hb 6.5 g/dl; lower row). First column: RUCT image ("RUCT"); second column: overlay of RUCT and color-coded signal visualization of MSOT signal at 700 nm ("700 nm", single wavelength); third column: overlay of RUCT and color-coded signal visualization of MSOT signal for HbR ("Hb", unmixed MSOT parameter). Scale bar (white) indicates 10 mm. (B-I) Quantitative analysis of MSOT signal intensity [au] for the unmixed MSOT parameter HbR (B-E) and the single wavelength 700 nm (F-I) based on measurements of the radial artery (VR5 and VR6) of patients. ROIs for quantitative signal analysis were drawn to encompass the vascular structure in the RUCT image in a blinded fashion with subsequent batch data analysis. The displayed groups include: "normal" (n = 6; Hb ≥ LLN and ≤ ULN; range 13.3 g/dl to 16.2 g/dl), "non-severe anemia" (n = 7; Hb ≥ 8 g/dl and < LLN; range 8.1 g/dl to 10.1 g/dl), and "severe anemia" (n = 6; Hb < 8 g/dl; range 4.5 g/dl to 7.6 g/dl). "Control" (n = 13, Hb ≥ 8 g/dl; range 8.1 g/dl to 16.2 g/dl) encompasses the subgroups "non-severe anemia" and "normal". (B) Graphic depiction of the MSOT signal level for the unmixed MSOT parameter HbR [au] on the y-axis and the groups "control" vs. "severe anemia" on the x-axis. Data are shown as truncated violin plot with depiction of individual values representing the mean of VR5 and VR6 for each patient. Statistical analysis by unpaired t-test (***$p < 0.001$; Power (1- β err prob) = 0.99). (C) Subgroup analysis with graphic depiction of the MSOT signal level for the unmixed MSOT parameter HbR [au] on the y-axis and the groups "normal" vs. "non-severe anemia" vs. "severe anemia" on the x-axis. Data are shown as truncated violin plot with depiction of individual values representing the mean of VR5 and VR6 for each patient. One-Way ANOVA with Tukey post-hoc test: "severe anemia" vs. "normal" (*$p < 0.05$); "severe anemia" vs. "non-severe anemia" (**$p < 0.01$). (D) Receiver operating characteristic (ROC) for the identification of "severe anemia" (n = 6) vs. "control" (n = 13) using the MSOT signal level [au] of the spectrally unmixed MSOT parameter HbR. Also given are the Area under the ROC curve (AUROC) with 0.9744 and the 95% confidence interval [0.9115–1.000]. (E) Graphic depiction of in vivo MSOT data [au] for the spectrally unmixed MSOT parameter HbR measured in the radial vascular regions VR5 and VR6. Data are shown as individual values representing the mean of VR5 and VR6 for each patient with an interpolated standard curve based on a sigmoidal curve-fitting approach. Correlation analysis was performed using Spearman's rank correlation coefficient with a resulting strong positive correlation (Spearman r 0.7034; 95% CI [0.3228–0.8882]; **$p < 0.01$). (F) Graphic depiction of the MSOT signal level for the single wavelength 700 nm [au] on the y-axis and the groups "control" vs. "severe anemia" on the x-axis. Data are shown as truncated violin plot with depiction of individual values representing the mean of VR5 and VR6 for each patient. Statistical analysis by unpaired t-test (***$p < 0.001$; Power (1- β err prob) = 0.99). (G) Subgroup analysis with graphic depiction of the MSOT signal level for the single wavelength 700 nm [au] on the y-axis and the groups "normal" vs. "non-severe anemia" vs. "severe anemia" on the x-axis. Data are shown as truncated violin plot with depiction of individual values representing the mean of VR5 and VR6 for each patient. One-Way ANOVA with Tukey post-hoc test: "severe anemia" vs. "normal" (*$p < 0.05$); "severe anemia" vs. "non-severe anemia" (**$p < 0.01$). (H) Receiver operating characteristic (ROC) for the identification of "severe anemia" (n = 6) vs. "control" (n = 13) using the MSOT signal level [au] of the single wavelength 700 nm. Also given are the Area under the ROC curve (AUROC) with 0.9872 and the 95% confidence interval [0.9472–1.000]. (I) Graphic depiction of in vivo MSOT data [au] for the single wavelength parameter 700 nm measured in the radial vascular regions VR5 and VR6. Data are shown as individual values representing the mean of VR5 and VR6 for each patient with an interpolated standard curve based on a sigmoidal curve-fitting approach. Correlation analysis was performed using Spearman's rank correlation coefficient with a resulting moderate positive correlation (Spearman r 0.5858; 95% CI [0.1312–0.8368]; *$p < 0.05$). (J-K) RUCT images visualizing the variable distance of the radial arteries in different patients from the body surface. Shown are the RUCT images from Fig. 5 A in magnification and with a depth scale [mm] measuring from the tissue surface (white arrow) which is directly in contact with the detector probe surface (white arrow head). The depth of the vessel is 2.2 mm (J) and 6.5 mm (K). Scale bar (white) indicates 10 mm. (L-M) Graphic depiction of in vivo MSOT data [au] for the spectrally unmixed MSOT parameter HbR (L) and the single wavelength 700 nm (M) for each radial vascular region separately on the y axis against the depth [mm] on the x-axis. Simple linear regression of MSOT signal intensity [au] vs. depth [mm] was performed with an additional correlation analysis (HbR: Pearson r 0.08590; R^2 0.007379; 95% CI [−0.2404 to 0.3947] and 700 nm: Pearson r − 0.04197; R^2 0.001762; 95% CI [−0.3569 to 0.2815].

**$p < 0.01$) and patients without anemia (*$p < 0.05$) (Fig. 5C). Receiver operating characteristic for severe anemia patients versus patients in the control group resulted in an excellent area under the curve (AUROC) of 0.9744 (95% CI [0.9115–1.000]; **$p < 0.01$; Fig. 5D). A standard curve fitted for MSOT signal intensity [au] for HbR and hemoglobin concentration [g/dl] over the full range of hemoglobin concentrations using a sigmoidal curve-fitting approach reflected a non-linear positive correlation. Spearman's rank correlation analysis confirmed a strong positive correlation (Spearman r 0.7034; 95% CI [0.3228–0.8882]; **$p < 0.01$; Fig. 5E).

In a next step, we evaluated whether a simplified single wavelength parameter analysis could also be utilized to identify patients with severe anemia (Fig. 5F-I). We found that MSOT signal intensity [au] at 700 nm also proved excellent in identifying patients with severe anemia versus the control group (***$p < 0.001$; Fig. 5F). Subgroup analysis using one-way ANOVA with Tukey's test again allowed distinguishing severely anemic patients reliably from patients with non-severe anemia (**$p < 0.01$) and patients with hemoglobin within the normal range (*$p < 0.05$; Fig. 5G). Accordingly, receiver operating characteristic of severe anemia patients versus patients in the control group resulted in an area under the curve (AUROC) in the same excellent range as for the spectrally unmixed HbR (700 nm: AUROC 0.9872 (95% CI [0.9472–1.000]; ***$p < 0.001$; Fig. 5H). Analogous to the unmixed HbR, a standard curve fitted for MSOT signal intensity [au] at 700 nm and hemoglobin concentration [g/dl] using a sigmoidal curve-fitting approach with additional correlation analysis yielded a non-linear moderately positive correlation (Spearman r 0.5858; 95% CI [0.1312–0.8368]; *$p < 0.05$; Fig. 5I).

While the radial arteries of our patients were all relatively superficial i.e., less than a centimeter below the tissue surface, there were relevant differences regarding the depth. Fig. 5J and K show the RUCT images of the patients from Fig. 5A magnified and with an additional scale bar. The radial artery of the patient with the normal range hemoglobin lies in a depth of 2.2 mm (Fig. 5 J), while the patient with severe anemia has a depth of 6.5 mm (Fig. 5K). Depth-dependent decay of light fluence impacts the optoacoustic signal intensity, however, an exponential correction was applied to the signal [11]. Therefore, we analyzed whether the depth of a targeted blood vessel would influence the MSOT signal intensity independently of the hemoglobin concentration. We found that MSOT signal intensity [au] for both HbR (Pearson r 0.08590; 95% CI [−0.2404 to 0.3947]; R^2 0.007379; ns $p \geq 0.05$; Fig. 5 L) and 700 nm (Pearson r − 0.04197; 95% CI [−0.3569 to 0.2815]; R^2 0.001762; ns $p \geq 0.05$; Fig. 5M) did not correlate with the depth of the vessel [mm].

In an extended analysis, we found that the spectrally unmixed composite parameter HbT was able to distinguish the patients with severe anemia from the control group and patients with non-severe anemia respectively (Fig. S4A, B) with an area under the curve (AUROC) for the first being 0.7949; 95% CI [0.5414–1.000]; *$p < 0.05$, Fig. S4C). However, there was only a weak positive correlation between MSOT signal and hemoglobin concentration (Spearman r 0.2160; 95% CI [-0.3094–0.6403]; ns $p \geq 0.05$); Fig. S4D). Interestingly, we found a possible explanation for this in form of the MSOT composite parameter HbT showing a moderate negative correlation between MSOT signal intensity and depth of the radial artery (Pearson r − 0.4186; R^2 0.1752; **$p < 0.01$; Fig. S4E) not observed for HbR. Similar findings were made with the spectrally unmixed MSOT parameter HbO_2 (Fig. S4F-J), which was not significantly different in between the different patient groups (Fig. S4F, G). Moreover, we found that for the single wavelength parameters 760 nm (Fig. S4K-O), 800 nm (Fig. S4 P-T), and 900 nm (Fig. S4U-Y) increasing wavelengths led to a deteriorating performance in distinguishing the study groups. Furthermore, we observed a

decreasing correlation of the MSOT signal and the hemoglobin concentration and, in turn, an increasing negative correlation of MSOT signal intensity and depth of the radial artery (Fig. S4).

Interestingly, using the additional parameter hematocrit, which reflects the volume density of RBCs in blood, we also found that the correlation of MSOT signal intensity at 700 nm with hematocrit (Spearman r 0.5719) is comparable to that with hemoglobin (Spearman r 0.5858) (Fig. S5A). The same was true for the correlation at 800 nm (Fig. S5B).

Regarding the other vascular regions, a lack of penetration depth with the current setup proved to be hindering in the inguinal region in which only 26 of the 38 vascular regions could be measured after identifying a vascular structure in an independent non-blinded analysis. While the jugular (37 out of 38 VRs successfully measured) and cubital (all 38 VRs successfully measured) regions did not have this problem, a lack of standardization due to highly variable vessel depths, several vessels (both veins and arteries) within the RUCT image, and common disturbances such as peripheral venous catheters and superficial hematoma as residuals from phlebotomy, contributed to a decreased performance compared to our radial artery focused analysis (Fig. S6A-C).

Overall, the signal intensity of the spectrally unmixed MSOT parameter HbR and the single wavelength parameter 700 nm measured in the radial vascular region proved to be highly accurate and reliable in identifying patients with severe anemia.

4. Discussion

Previous in vivo studies have employed animal models for technical validation of the employed optoacoustic imaging system, finding that optoacoustic imaging was able to detect changes in blood oxygenation and to assess the distribution of a contrast agent [12]. Changes in oxygenation were also used to assess perfusion of cancerous lesions in animal models in vivo [13]. Further in vitro studies substantiated a good correlation between optoacoustic measurements with laboratory determined total hemoglobin [14]. Hence, these and other studies [15,16] suggested that optoacoustic imaging might be a feasible approach to quantify hemoglobin in patients in vivo.

Based on recent technical advancements, optoacoustic imaging (OAI) is quickly establishing itself as a highly promising approach in biomedicine with a broad spectrum of possible applications. Multispectral optoacoustic tomography (MSOT) has already been employed for high-resolution imaging of structures such as blood vessels both ex vivo and in vivo, based on qualitative measurements of endogenous fluorophores including melanin, as well as hemoglobin, both oxygenated and deoxygenated [2,4,17,18].

In clinical studies, label-free MSOT imaging signal intensities of endogenous molecules such as collagen in patients with Duchenne muscular dystrophy [3] or hemoglobin in patients with inflammatory bowel disease [5,6] have recently been used as surrogate parameters for assessing disease severities of degenerative and inflammatory conditions. Along the same lines, relative changes of hemoglobin as surrogate marker of perfusion have been correlated to disease severity in psoriatic arthritis [19], peripheral artery disease [20], and others [21,22].

In our current translational study, we first evaluated the general technical feasibility of a (semi-) quantitative hemoglobin measurement by performing fine-grained dilution series of whole blood in plasma isotone saline ex vivo and measuring it with the latest generation of an integrated MSOT clinical research device. In this, we could substantiate a strong positive monotonic non-linear correlation of MSOT signal intensity and absolute hemoglobin concentration for both single wavelength parameters and spectrally unmixed MSOT parameters. Importantly, even with a limited amount of training data, MSOT signal intensity at 800 nm measured ex vivo could be used to adequately interpolate the absolute hemoglobin concentration in unknown test samples with high precision. These results represented an encouraging first step in determining the feasibility of quantitative MSOT analysis of hemoglobin in vivo. Additionally, our preclinical experiments comparatively using an isotone (saline) or hypotonic (water) dilution medium confirmed a previous observation that tonicity affects absolute signal intensity in photoacoustic measurements of the hemoglobin molecule while encased in erythrocytes [23]. Explanation for the reduced absolute signal intensity when using hypotonic solutions is plausibly the quelling of erythrocytes leading to a reduced density of the hemoglobin molecule within a defined measurement region, as has been observed by Gorey and colleagues in a continuous-wave photoacoustic measurement setting [23].

To translate our findings into the clinical setting, we next devised an exploratory proof-of-concept study evaluating MSOT signal intensity measured with our same advanced MSOT clinical research device in the blood vessels of patients with normal hemoglobin concentration and different severities of anemia in vivo in a total of 19 patients. Importantly, our MSOT approach proved excellent in identifying patients with severe anemia based on a strong positive correlation of MSOT signal intensity for the unmixed MSOT parameter HbR and the single wavelength 700 nm with absolute hemoglobin concentration. In contrast to our ex vivo results, the MSOT parameter HbR and the single wavelength 700 nm were highly superior regarding their discriminatory capability between study groups, as well as the strength of their positive correlation with absolute hemoglobin concentration in vivo. We explain these findings by penetration depth-dependent wavelength-specific absorption properties of the surrounding tissue in vivo, as evidenced by our data presented in Fig. S4. Accordingly, we reason that the superiority of HbR and 700 nm might be due to the fact that both are non-dependent on the measurement depth in tissue in the relevant range of e.g., the radial vascular region due to the absorption properties of the overlying tissue. Our analysis was further aided by the fact that all patients had an oxygen saturation in the normal range, leaving the difference of deoxyhemoglobin in an arterial vessel negligible. While our findings regarding the correlation of MSOT signal intensity and hematocrit complement and confirm our ex vivo findings using a hypotonic dilution medium, hematocrit alone is not an established parameter in the diagnosis of anemia in clinical medicine and there is no subgroup stratification of anemia severity (non-severe vs. severe) based on hematocrit. Therefore, although very important from a methodical and technical perspective, using hemoglobin offers more granularity and a superior performance as a diagnostic test as it allows to identify patients with severe anemia benefitting from RBC transfusion.

Regarding our technical setup, we found that a visually determined region-of-interest (ROI) led to increased absolute measurement values compared to a standardized geometric ROI in the ex vivo samples due to the fact that we chose a mean pixel intensity analysis. While this approach results in variability conditioned by the element of human input in the process of devising the ROI ex vivo, new algorithm-based techniques could reliably replace this step, facilitating faster and automated analysis. Alternative approaches would be an adapted smaller geometry of the sample container to prevent relevant signal absorption/attenuation or an alternative mode of analysis (e.g., top-ten-pixel analysis). However, this limitation only applies to ex vivo samples as our in vivo determination of ROIs was based exclusively on the anatomical structures of the blood vessels as imaged via RUCT. In this regard, a general limitation of the in vivo study was, that some of the vascular regions e.g., inguinal, could not be properly imaged with the current device, as the relevant blood vessels in those regions lay too deep and were therefore out of focus. We speculate that the current setup might be limited to a depth of around 20 mm for accurate analysis. However, it is important to emphasize that the configuration i.e., hemoglobin content of the overlying tissue (e.g., muscle tissue versus adipose tissue) is also a relevant determinant of the maximum achievable depth suitable for analysis. In other regions such as the cubital, interindividual highly variable anatomy and several blood vessels including both arteries and veins within the imaging area hampered standardization. Importantly, basing our analysis on the radial vascular region largely avoided these problems and resulted in a reliably detectable and identifiable vascular

structure, the radial artery, via RUCT within adequate measurement depth for all our patients, which in our cohort did not exceed 7 mm from the skin. We observed that our ex vivo data resulted in very strong correlation between MSOT signal intensity and hemoglobin concentration, while our in vivo data offered strong correlations. In particular MSOT signal intensity increased over the complete range of hemoglobin concentration ex vivo from 0 to > 16 g/dl, while in vivo there was a ceiling effect around a hemoglobin concentration of 9–10 g/dl. We speculate that these discrepancies might be explained the different experimental settings. First, blood outside of the body drawn from a vein will have a different ratio of oxygenated to deoxygenated hemoglobin as compared to the in vivo setting in an artery. This will impact wavelength-dependent light fluence and may impact the sensitivity of spectral unmixing. Second, in vivo measurements occur within a heterogenous tissue background, which also has an unpredictable impact on spectral unmixing. Taken together, these differences make a comparison of ex vivo to in vivo studies difficult to interpret. The nonlinear relationship of MSOT HbR and hemoglobin concentration with existence of a ceiling effect for higher hemoglobin concentrations in vivo has implications for clinical decision making as well. Optoacoustic hemoglobin quantification with the current system could therefore be a highly useful clinical tool for quickly ruling out severe anemia in emergency care settings or serve as a longitudinal monitoring system to detect severe drops in hemoglobin necessitating transfusion e.g., in the ICU. Technically, the size of the vessels does impact the signal intensity, mainly due to decay of light fluence along depth. The blood on the proximal side of the vessel reduces light penetration and leads to decreased fluence at depth. This could be partially solved by e.g., drawing superficial ROIs (as we demonstrated with the visual ROIs ex vivo). However, larger vessels are usually located at deeper parts of the body, which also contributes to the fluence issue. In this study, a fluence correction was applied on the scans assuming an exponential decay of fluence along depth [11]. In the future, more accurate models of fluence correction could contribute to accurate quantification of signal at depth.

This underscores the importance of developing tissue segmentation algorithms specific to our particular indication to improve spectral unmixing. Importantly, single wavelength analysis at 700 nm and in general proved to be non-inferior to spectrally unmixed MSOT parameters in our analysis, suggesting the feasibility of less complex, possibly handheld and portable devices for this purpose in the future.

While photoplethysmographic methods in screening settings [24] and non-invasive assessment of hemoglobin based on spectrophotometry in CO pulse oximeters have been used as a rather accurate screening tool for blood donors [25] and patients with anemia due to trauma [26], studies including severely ill patients with e.g., circulatory shock, on vasopressor treatment, and in intensive care units have shown the limits of this technological approach [27]. This is similar to the restrictions described for classical pulse oximeters in patients with severe sepsis and septic shock, in which hypoxemia represents an additional and independent factor leading to overestimation of blood oxygen saturation [28]. In an important distinction, our methodical approach focusing on hemoglobin quantification via larger blood vessels e.g., the radial artery, would not be prone to limitations caused by these factors. In this context, follow-up studies will create a better understanding if vascular pathologies (i.e., severe atherosclerosis) and/or conditions significantly altering the composition of the blood (i.e., hypertriglyceridemia, hyperglycemia, etc.) interfere with MSOT measurements of hemoglobin. Importantly, follow-up studies will also need to assess to what extent different skin tones i.e., differing quantities of melanin, the major optical absorber in the skin, affect the in vivo measurements of hemoglobin in our setup. Mantri and Jokerst have previously demonstrated the effect of skin tone on multiple photoacoustic measurement parameters [29]. To address this potential issue, both using technical correction factors and/or subgroup specific normal values might be employed. To the best of our knowledge, our study for the first time provides insight into the capabilities of the current generation of multispectral optoacoustic imaging devices for absolute quantitative assessment of hemoglobin in patients in vivo. While absolute quantification of hemoglobin by MSOT signal intensity proved highly accurate in our ex vivo measurement setting, our in vivo measurements faced known challenges of optoacoustic quantification in tissues. As Regensburger and colleagues recently reviewed [30], improving quantification of optoacoustic imaging is a rapidly evolving topic [11,31]. Importantly, while most quantitative optoacoustic studies so far have used exogenous compounds [32,33], a recent study by Hysi and colleagues took an approach comparable to ours by quantifying collagen using photoacoustic imaging in a kidney fibrosis model [34]. Following preclinical experiments, the authors conducted successful ex vivo optoacoustic fibrosis quantification of human kidneys providing compelling evidence for the potential value of quantitative optoacoustic imaging in evaluating the quality of explanted donor kidneys in transplant medicine. However, the authors correctly point out, that despite recent advances ([6,35,36]), tissue imaging particularly in deeper seated organs in vivo remains an important unsolved problem. Accordingly, in our study, depth prevented measurements in e.g., the inguinal blood vessels in a majority of patients. However, the depth of the radial artery, the main access point for sample drawing for arterial blood gas analysis (aBG) and catheterization, was within focus in all our patients. Thereby, we were able to demonstrate semiquantitative analysis as an important milestone in frame of the further development of MSOT-based quantitative hemoglobin measurement as a novel diagnostic tool for the prompt and reliable diagnosis of severe anemia in vivo.

In a future clinical perspective, our study lays the foundation for the integration of quantitative hemoglobin analysis into multispectral optoacoustic imaging in both preclinical and clinical studies. While our approach is already able to identify a blood transfusion triggering degree of severe anemia in vivo today, making it, for example, a useful tool for non-invasive longitudinal monitoring of ICU patients or patients in the OR, technical refinements and optimizations will be necessary to achieve the same accuracy already available in our ex vivo measurements. Furthermore, by technically addressing tissue depth and absorption issues, other blood vessel regions might become accessible for measurement. Another aspect of this is that our current in vivo measurement setup is mainly based on the analysis of the depth independent parameters HbR and 700 nm, creating a possible dependency on the oxygen saturation of the measured arterial blood. In patients suffering from a combination of anemia (low hemoglobin) with concurrent oxygenation impairment (e.g., respiratory failure) this might impair accurate results. To address this potential issue, a wavelength-specific depth correction factor of MSOT signal intensity might allow a depth independent signal evaluation for e.g., HbT or 800 nm, either as substitute parameters for our current parameters (700 nm, HbR), or in form of a correctional factor. This appears feasible especially considering that the negative correlation between MSOT signal intensity and hemoglobin concentration, which increases with longer wavelengths, appears to be linear. An alternative yet more complex avenue would be to develop algorithms addressing the tissue specific absorption on the level of signal reconstruction. Follow-up studies incorporating new engineering advancements will be necessary to evaluate the practical feasibility of these concepts in improving the capabilities of our MSOT platform for quantification of hemoglobin and its oxygen saturation in the clinical setting.

Finally, local quantitative perfusion assessment is another promising potential field of application. Promisingly, previous studies were already able to demonstrate a positive correlation of foot perfusion assessed by general optoacoustic signal intensity in pedal tissue of dialysis patients and healthy controls with systolic blood pressure [37]. Real-time local quantitative perfusion and oxygenation analysis based on quantitative assessment of oxygenated and deoxygenated hemoglobin could prove valuable in numerous settings, including assessing perfusion of a freshly implanted kidney as an addition to pulse doppler sonography on a tissue level, and in support of both preclinical and clinical functional imaging studies in various tissues.

Funding

No external funding sources.

Data Availability

All data are available in the main text or the Supplementary materials and are available upon reasonable request.

Acknowledgments

The Interdisciplinary Center for Clinical Research (IZKF) Erlangen supported I.G. through participation in the Clinician-Scientist-Program. The present work was performed in partial fulfillment of the requirements for obtaining the degree "Dr. med." for W.H. at the Friedrich-Alexander-University Erlangen-Nürnberg (FAU). We thank Yi Qiu (iThera Medical GmbH) for assistance with data analysis and statistical analysis. We thank Florian Fuchs, Sabine Zirlik, Inka Hübner, and Tomislav Vilusic for logistical support, and Daniel Beß for excellent technical support.

Competing interests

The authors declare the following financial interests/personal relationships which may be considered as potential competing interests: Maximilian J. Waldner reports administrative support, equipment, drugs, or supplies, statistical analysis, and writing assistance were provided by iThera Medical GmbH. Maximilian J. Waldner has patent #EP3937755A1 pending to Ithera Medical GmbH Friedrich Alexander Univeritaet Erlangen Nuernberg FAU. MJW is co-inventor together with iThera Medical GmbH, Germany on an EU patent application (EP 19 163 304.9) relating to a device and a method for analyzing optoacoustic data, an optoacoustic system and a computer program.

Appendix A. Supporting information

Supplementary data associated with this article can be found in the online version at doi:10.1016/j.pacs.2022.100414.

References

[1] J. Chen, Y. Fang, L. Sun, F. Zeng, S. Wu, An activatable probe for detecting alcoholic liver injury via multispectral optoacoustic tomography and fluorescence imaging, Chem. Commun. 56 (75) (2020) 11102–11105.
[2] I. Stoffels, S. Morscher, I. Helfrich, U. Hillen, J. Leyh, N.C. Burton, T.C. Sardella, J. Claussen, T.D. Poeppel, H.S. Bachmann, A. Roesch, K. Griewank, D. Schadendorf, M. Gunzer, J. Klode, Metastatic status of sentinel lymph nodes in melanoma determined noninvasively with multispectral optoacoustic imaging, Sci. Transl. Med 7 (317) (2015) 317ra199.
[3] A.P. Regensburger, L.M. Fonteyne, J. Jungert, A.L. Wagner, T. Gerhalter, A. M. Nagel, R. Heiss, F. Flenkenthaler, M. Qurashi, M.F. Neurath, N. Klymiuk, E. Kemter, T. Frohlich, M. Uder, J. Woelfle, W. Rascher, R. Trollmann, E. Wolf, M. J. Waldner, F. Knieling, Detection of collagens by multispectral optoacoustic tomography as an imaging biomarker for Duchenne muscular dystrophy, Nat. Med 25 (12) (2019) 1905–1915.
[4] G. Diot, S. Metz, A. Noske, E. Liapis, B. Schroeder, S.V. Ovsepian, R. Meier, E. Rummeny, V. Ntziachristos, Multispectral optoacoustic tomography (MSOT) of human breast cancer, Clin. Cancer Res 23 (22) (2017) 6912–6922.
[5] M.J. Waldner, F. Knieling, C. Egger, S. Morscher, J. Claussen, M. Vetter, C. Kielisch, S. Fischer, L. Pfeifer, A. Hagel, R.S. Goertz, D. Wildner, R. Atreya, D. Strobel, M. F. Neurath, Multispectral optoacoustic tomography in Crohn's disease: noninvasive imaging of disease activity, Gastroenterology 151 (2) (2016) 238–240.
[6] F. Knieling, C. Neufert, A. Hartmann, J. Claussen, A. Urich, C. Egger, M. Vetter, S. Fischer, L. Pfeifer, A. Hagel, C. Kielisch, R.S. Gortz, D. Wildner, M. Engel, J. Rother, W. Uter, J. Siebler, R. Atreya, W. Rascher, D. Strobel, M.F. Neurath, M. J. Waldner, Multispectral optoacoustic tomography for assessment of Crohn's disease activity, N. Engl. J. Med 376 (13) (2017) 1292–1294.
[7] I. Olefir, S. Tzoumas, H. Yang, V. Ntziachristos, A. Bayesian, Approach to eigenspectra optoacoustic tomography, IEEE Trans. Med Imaging 37 (9) (2018) 2070–2079.
[8] S. Tzoumas, A. Nunes, I. Olefir, S. Stangl, P. Symvoulidis, S. Glasl, C. Bayer, G. Multhoff, V. Ntziachristos, Eigenspectra optoacoustic tomography achieves quantitative blood oxygenation imaging deep in tissues, Nat. Commun. 7 (2016) 12121.
[9] F. Faul, E. Erdfelder, A.G. Lang, A. Buchner, G*Power 3: a flexible statistical power analysis program for the social, behavioral, and biomedical sciences, Behav. Res Methods 39 (2) (2007) 175–191.
[10] F. Faul, E. Erdfelder, A. Buchner, A.G. Lang, Statistical power analyses using G*Power 3.1: tests for correlation and regression analyses, Behav. Res Methods 41 (4) (2009) 1149–1160.
[11] F.M. Brochu, J. Brunker, J. Joseph, M.R. Tomaszewski, S. Morscher, S.E. Bohndiek, Towards quantitative evaluation of tissue absorption coefficients using light fluence correction in optoacoustic tomography, IEEE Trans. Med. Imaging 36 (1) (2017) 322–331.
[12] J. Joseph, M.K. Ajith Singh, N. Sato, S.E. Bohndiek, Technical validation studies of a dual-wavelength LED-based photoacoustic and ultrasound imaging system, Photoacoustics 22 (2021), 100267.
[13] M.R. Tomaszewski, I.Q. Gonzalez, J.P. O'Connor, O. Abeyakoon, G.J. Parker, K. J. Williams, F.J. Gilbert, S.E. Bohndiek, Oxygen enhanced optoacoustic tomography (OE-OT) reveals vascular dynamics in murine models of prostate cancer, Theranostics 7 (11) (2017) 2900–2913.
[14] L. Hacker, J. Brunker, E.S.J. Smith, I. Quiros-Gonzalez, S.E. Bohndiek, Photoacoustics resolves species-specific differences in hemoglobin concentration and oxygenation, J. Biomed. Opt. 25 (9) (2020).
[15] R.O. Esenaliev, Y.Y. Petrov, O. Hartrumpf, D.J. Deyo, D.S. Prough, Continuous, noninvasive monitoring of total hemoglobin concentration by an optoacoustic technique, Appl. Opt. 43 (17) (2004) 3401–3407.
[16] I.Y. Petrova, R.O. Esenaliev, Y.Y. Petrov, H.P. Brecht, C.H. Svensen, J. Olsson, D. J. Deyo, D.S. Prough, Optoacoustic monitoring of blood hemoglobin concentration: a pilot clinical study, Opt. Lett. 30 (13) (2005) 1677–1679.
[17] A. Karlas, M. Kallmayer, M. Bariotakis, N.A. Fasoula, E. Liapis, F. Hyafil, J. Pelisek, M. Wildgruber, H.H. Eckstein, V. Ntziachristos, Multispectral optoacoustic tomography of lipid and hemoglobin contrast in human carotid atherosclerosis, Photoacoustics 23 (2021), 100283.
[18] M. Masthoff, A. Helfen, J. Claussen, A. Karlas, N.A. Markwardt, V. Ntziachristos, M. Eisenblatter, M. Wildgruber, Use of multispectral optoacoustic tomography to diagnose vascular malformations, JAMA Dermatol. 154 (12) (2018) 1457–1462.
[19] S. Hallasch, N. Giese, I. Stoffels, J. Klode, W. Sondermann, Multispectral optoacoustic tomography might be a helpful tool for noninvasive early diagnosis of psoriatic arthritis, Photoacoustics 21 (2021), 100225.
[20] A. Karlas, M. Masthoff, M. Kallmayer, A. Helfen, M. Bariotakis, N.A. Fasoula, M. Schafers, M. Seidensticker, H.H. Eckstein, V. Ntziachristos, M. Wildgruber, Multispectral optoacoustic tomography of peripheral arterial disease based on muscle hemoglobin gradients-a pilot clinical study, Ann. Transl. Med 9 (1) (2021) 36.
[21] M. Masthoff, A. Helfen, J. Claussen, W. Roll, A. Karlas, H. Becker, G. Gabriels, J. Riess, W. Heindel, M. Schafers, V. Ntziachristos, M. Eisenblatter, U. Gerth, M. Wildgruber, Multispectral optoacoustic tomography of systemic sclerosis, J. Biophoton. 11 (11) (2018), e201800155.
[22] W. Roll, N.A. Markwardt, M. Masthoff, A. Helfen, J. Claussen, M. Eisenblatter, A. Hasenbach, S. Hermann, A. Karlas, M. Wildgruber, V. Ntziachristos, M. Schafers, Multispectral optoacoustic tomography of benign and malignant thyroid disorders: a pilot study, J. Nucl. Med. 60 (10) (2019) 1461–1466.
[23] A. Gorey, D. Biswas, A. Kumari, S. Gupta, N. Sharma, G.C.K. Chen, S. Vasudevan, Application of continuous-wave photoacoustic sensing to red blood cell morphology, Lasers Med Sci. 34 (3) (2019) 487–494.
[24] S. Acharya, D. Swaminathan, S. Das, K. Kansara, S. Chakraborty, R.D. Kumar, T. Francis, K.R. Aatre, Non-invasive estimation of hemoglobin using a multi-model stacking regressor, IEEE J. Biomed. Health Inf. 24 (6) (2020) 1717–1726.
[25] M. Al-Khabori, A.Z. Al-Riyami, K. Al-Farsi, M. Al-Huneini, A. Al-Hashim, N. Al-Kemyani, S. Daar, Validation of a non-invasive pulse CO-oximetry based hemoglobin estimation in normal blood donors, Transfus. Apher. Sci. 50 (1) (2014) 95–98.
[26] M. Gamal, B. Abdelhamid, D. Zakaria, O.A.E. Dayem, A. Rady, M. Fawzy, A. Hasanin, Evaluation of noninvasive hemoglobin monitoring in trauma patients with low hemoglobin levels, Shock 49 (2) (2018) 150–153.
[27] L.J. Moore, C.E. Wade, L. Vincent, J. Podbielski, E. Camp, D.D. Junco, H. Radhakrishnan, J. McCarthy, B. Gill, J.B. Holcomb, Evaluation of noninvasive hemoglobin measurements in trauma patients, Am. J. Surg. 206 (6) (2013) 1041–1047.
[28] B.J. Wilson, H.J. Cowan, J.A. Lord, D.J. Zuege, D.A. Zygun, The accuracy of pulse oximetry in emergency department patients with severe sepsis and septic shock: a retrospective cohort study, BMC Emerg. Med. 10 (2010) 9.
[29] Y. Mantri, J.V. Jokerst, Impact of skin tone on photoacoustic oximetry and tools to minimize bias, Biomed. Opt. Express 13 (2) (2022) 875–887.
[30] A.P. Regensburger, E. Brown, G. Kronke, M.J. Waldner, F. Knieling, Optoacoustic Imaging in Inflammation, Biomedicines 9 (5) (2021).
[31] J. Joseph, M.R. Tomaszewski, I. Quiros-Gonzalez, J. Weber, J. Brunker, S. E. Bohndiek, Evaluation of precision in optoacoustic tomography for preclinical imaging in living subjects, J. Nucl. Med 58 (5) (2017) 807–814.
[32] T. Anani, A. Brannen, P. Panizzi, E.C. Duin, A.E. David, Quantitative, real-time in vivo tracking of magnetic nanoparticles using multispectral optoacoustic tomography (MSOT) imaging, J. Pharm. Biomed. Anal. 178 (2020), 112951.
[33] A. Buehler, E. Herzog, D. Razansky, V. Ntziachristos, Video rate optoacoustic tomography of mouse kidney perfusion, Opt. Lett. 35 (14) (2010) 2475–2477.
[34] E. Hysi, X. He, M.N. Fadhel, T. Zhang, A. Krizova, M. Ordon, M. Farcas, K.T. Pace, V. Mintsopoulos, W.L. Lee, M.C. Kolios, D.A. Yuen, Photoacoustic imaging of kidney fibrosis for assessing pretransplant organ quality, JCI Insight 5 (10) (2020).

[35] L. Lin, P. Hu, J. Shi, C.M. Appleton, K. Maslov, L. Li, R. Zhang, L.V. Wang, Single-breath-hold photoacoustic computed tomography of the breast, Nat. Commun. 9 (1) (2018) 2352.
[36] L. Lin, X. Tong, P. Hu, M. Invernizzi, L. Lai, L.V. Wang, Photoacoustic computed tomography of breast cancer in response to neoadjuvant chemotherapy, Adv. Sci. 8 (7) (2021) 2003396.
[37] Y. Mantri, T.R. Dorobek, J. Tsujimoto, W.F. Penny, P.S. Garimella, J.V. Jokerst, Monitoring peripheral hemodynamic response to changes in blood pressure via photoacoustic imaging, Photoacoustics 26 (2022), 100345.

Ingo Ganzleben: Ingo Ganzleben, a physician scientist from the Department of Medicine 1, University Hospital Erlangen, Germany, is currently a postdoctoral fellow at Massachusetts General Hospital in Boston, USA. His basic and clinical research focuses on deciphering biological processes employing versatile imaging techniques.

Maximilian J. Waldner: Maximilian J. Waldner is a physician scientist at the Department of Medicine 1, University Hospital Erlangen, Germany. He is an attending and a full professor for functional imaging in medicine with a particular focus on clinical imaging studies.